Suppporting Information

Tuning the Nucleophilicity of Electron-Rich Diborane(4) Compounds with Bridging Guanidinate Substituents by Substitution

Julian Horn, Anna Widera, Sebastian Litters, Elisabeth Kaifer, Hans-Jörg Himmel*

Experimental Details for $[(i\mathrm{Pr})_3\mathrm{SiCCB}(\mu\text{-hpp})]_2$ (6)

NMR spectra for proton transfer reaction of $\{[(\mathrm{Me_2HN})\mathrm{B}(\mu\text{-hpp})]_2\}^{2+}$ and $[\mathrm{HB}(\mu\text{-hpp})]_2$

Analytical data for all new compounds

Summary of quantum chemical computations

Experimental Details for [(*i*Pr)$_3$SiCCB(μ-hpp)]$_2$ (6)

[TfOB(μ-hpp)]$_2$ (**4**, 253 mg, 0.424 mmol) was suspended in 8 ml of absolute THF. Lithiumtriisopropylsilylacetylide (170 mg, 0.934 mmol) in 1 ml THF was added. After stirring the clear, yellow reaction mixture for 30 minutes the solvent was removed in vacuo. The resulting residue was washed with methanol (5x3 ml), toluene (5x3 ml) and *n*-pentane (3x3 ml) and evaporated to dryness. After addition of 1 ml of dichloromethane and storage at −35 °C overnight, colorless crystals suitable for X-ray analysis formed. The still present impurities hampered the isolation of the compound in pure form. ^{1}H NMR (400 MHz, CD_2Cl_2): δ = 3.34−3.03 (m, 16H, N-C*H*$_2$), 1.94−1.77 (m, 8H, C*H*$_2$), 1.01 (d, *J* = 7.4 Hz, 18H, C*H*$_3$), 0.84 (sxt, *J* = 7.2 Hz, 3H, C*H*) ppm. ^{11}B NMR (128 MHz, CD_2Cl_2): δ = −5.75 (s, 2*B*, **6**) ppm. ^{11}B{^{1}H} NMR (128 MHz, CD_2Cl_2): δ = −5.75 (s, 2*B*) ppm. ^{13}C NMR (100 MHz, CD_2Cl_2): δ = 158.1 (*C*q), 109.5 ((*i*Pr)$_3$Si-*C*), 47.0 (N-*C*H$_2$), 41.4 (N-*C*H$_2$), 22.5 (*C*H$_2$), 18.6 (*C*H$_3$), 11.9 (*C*H) ppm. ^{29}Si NMR (80 MHz, CD_2Cl_2): δ = −7.29. MS (EI$^+$): m/z (%) = 660.5 ([M]$^+$, 100%), 617.5 ([M−*i*Pr]$^+$, 24%), 503.4 ([M−TIPS]$^+$, 11%), 479.4 ([M−CCTIPS]$^+$, 12%). Crystal data for **6**, M_r = 688.54, 0.50 x 0.20 x 0.15 mm, monoclinic, space group $P2_1$/c (*IT* Nr. 14), *a* = 15.046(3), *b* = 20.895(4), *c* = 28.002(6) Å, *V* = 8746.85 Å^3, *Z* = 8, ρ_{cald} = 1.046 Mg m^{-3}, Mo-K_α radiation (graphite-monochromated, λ = 0.71073 Å), *T* = 120 K, θ_{range} 2.1 to 27.5°. Reflections measured 19997, independent reflections 6862. R_{int} = 0.3002. Final *R* indices [$I > 2\sigma(I)$]: R_1 = 0.1048, wR_2 = 0.2892.

Proton transfer reaction between $\{[Me_2HNB(\mu\text{-hpp})]_2\}^{2+}$ and $[HB(\mu\text{-hpp})]_2$.

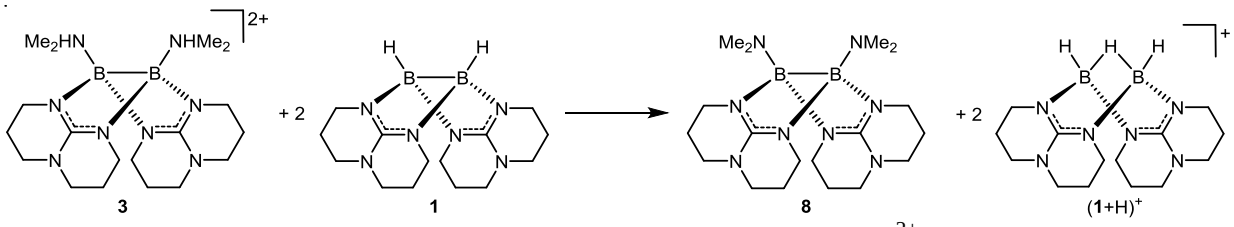

Scheme S1. Proton transfer reaction between $\{[Me_2HNB(\mu\text{-hpp})]_2\}^{2+}$ (**3**) and $[HB(\mu\text{-hpp})]_2$ (**1**).

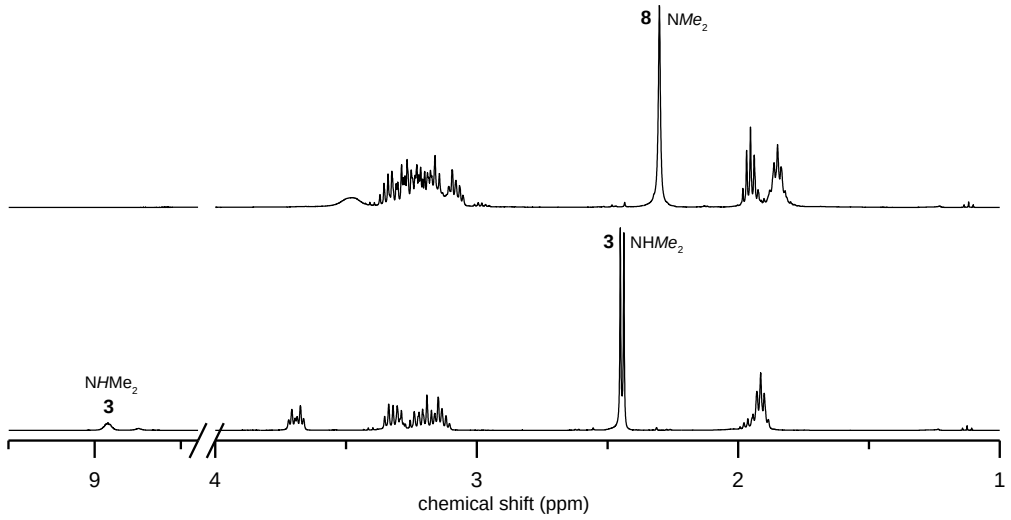

Figure S2. ^{1}H NMR spectra (CD_2Cl_2, 399.89 MHz) of the reactant **3** (bottom) and the mixture of **8** and (**1**+H)$^+$ obtained upon reaction between **1** and **3** (top). Characteristic peaks are assigned.

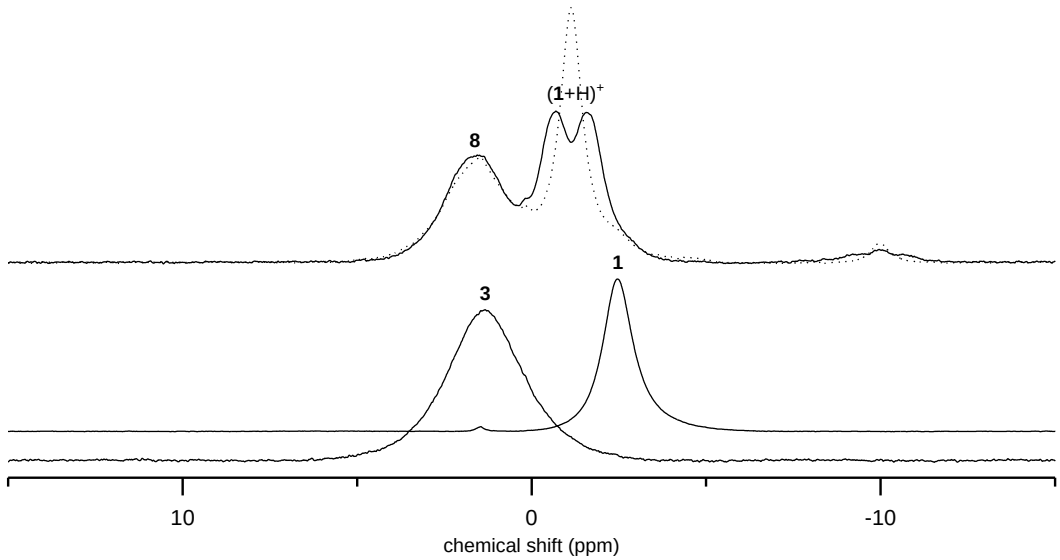

Figure S3. ^{11}B NMR spectra (CD_2Cl_2, 128.30 MHz) of the reactants **3** and **1** (bottom) and the mixture of **8** and (**1**+H)$^+$ obtained upon reaction between **1** and **3** (top). Dashed lines show the $^{11}B\{^1H\}$ NMR spectrum. Characteristic peaks are assigned.

Analytical data for all new compounds

1) [TfOB(μ-hpp)]$_2$ (4)

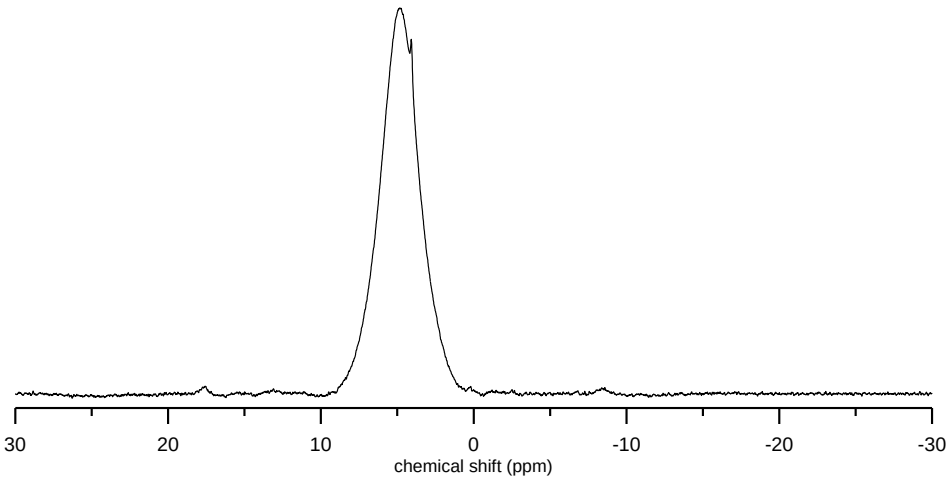

Figure S4. ^{11}B NMR spectrum (CD_2Cl_2, 128.30 MHz) for **4**.

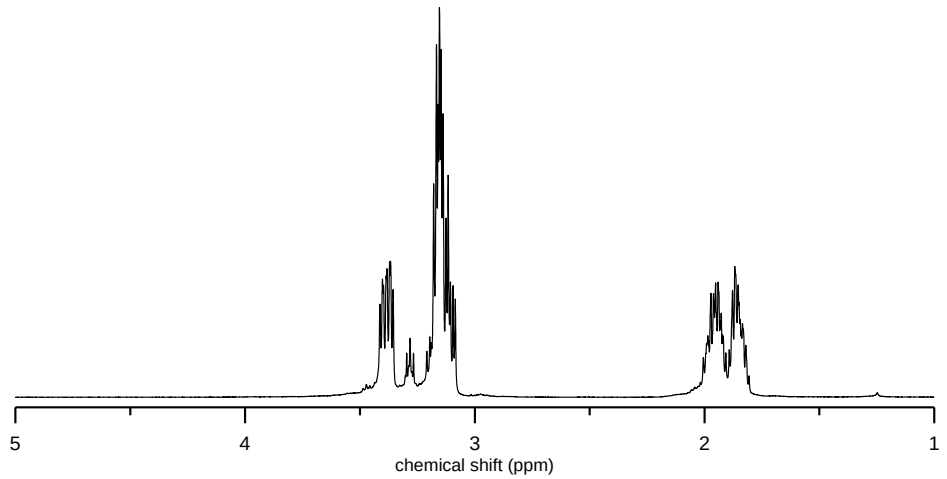

Figure S5. ^{1}H NMR spectrum (CD_2Cl_2, 399.89 MHz) for **4**.

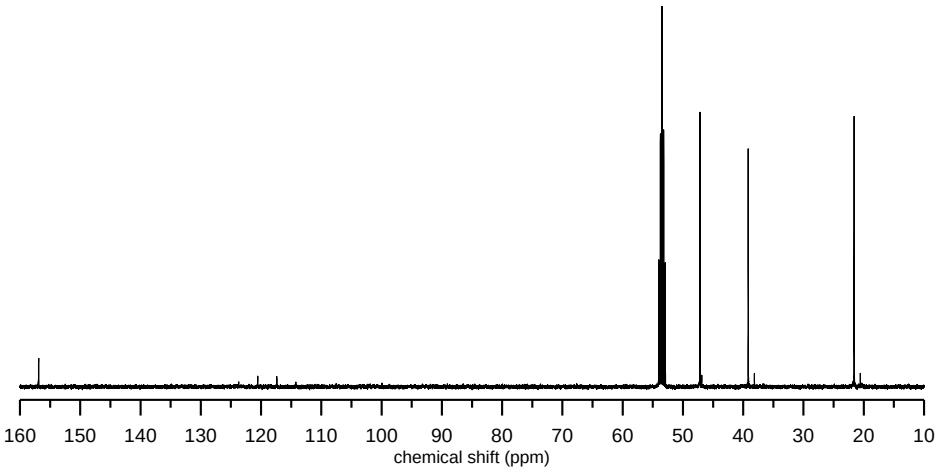

Figure S6. ^{13}C NMR (CD_2Cl_2, 100.55 MHz) for **4**.

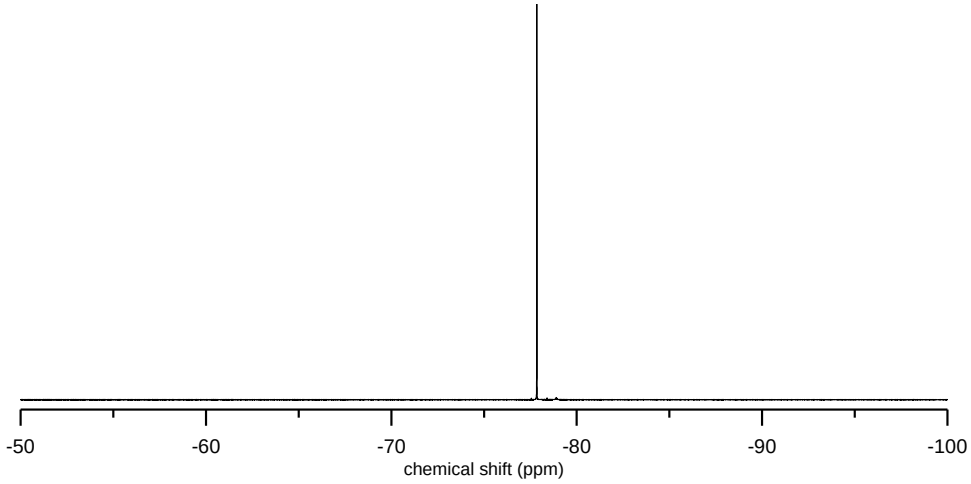

Figure S7. ^{19}F NMR spectrum (CD_2Cl_2, 376.27 MHz) for **4**.

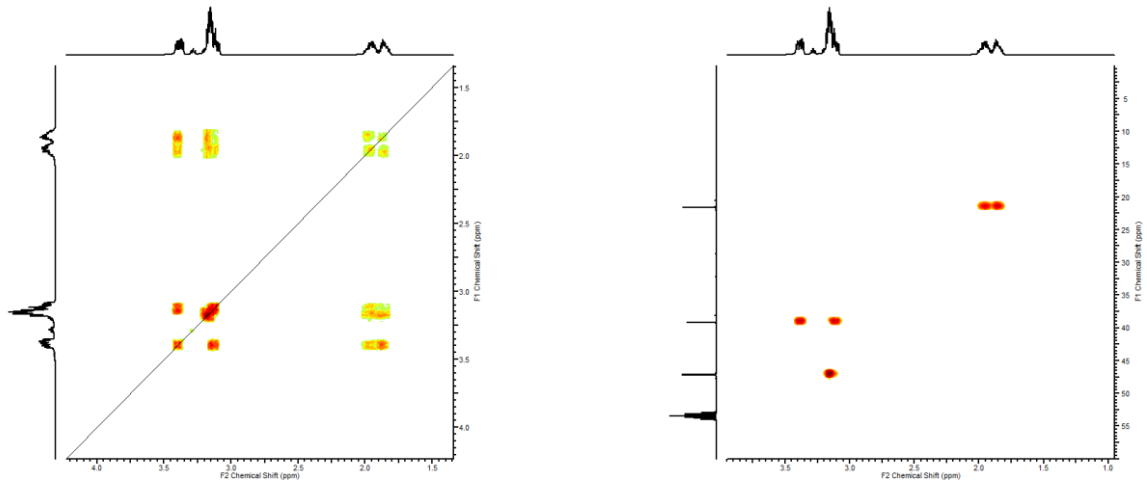

Figure S8. ^{1}H/^{1}H COSY-NMR spectrum (CD_2Cl_2, 399.89/399.89 MHz, left) and ^{1}H/^{13}C HSQC-NMR spectrum (CD_2Cl_2, 399.89/100.56 MHz, right) for **4**.

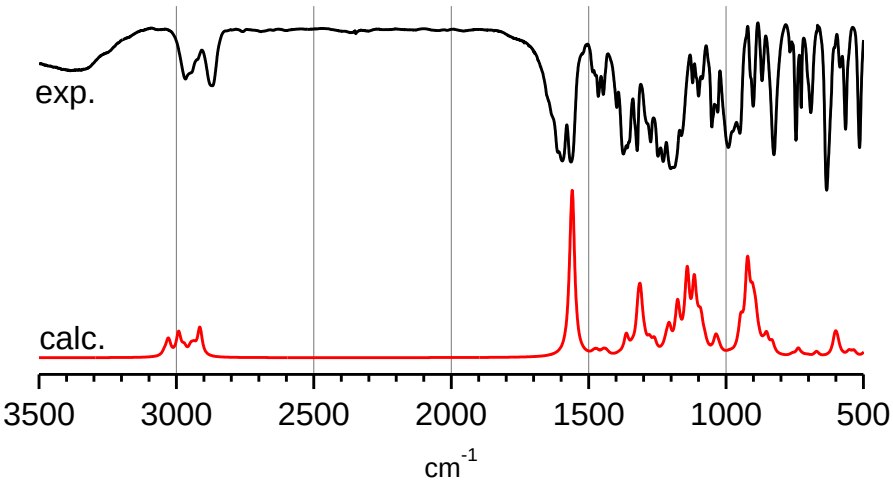

Figure S9. Experimental (KBr, top) and calculated (B3LYP-D3/def2-TZVPP, bottom) IR-spectra of **4**.

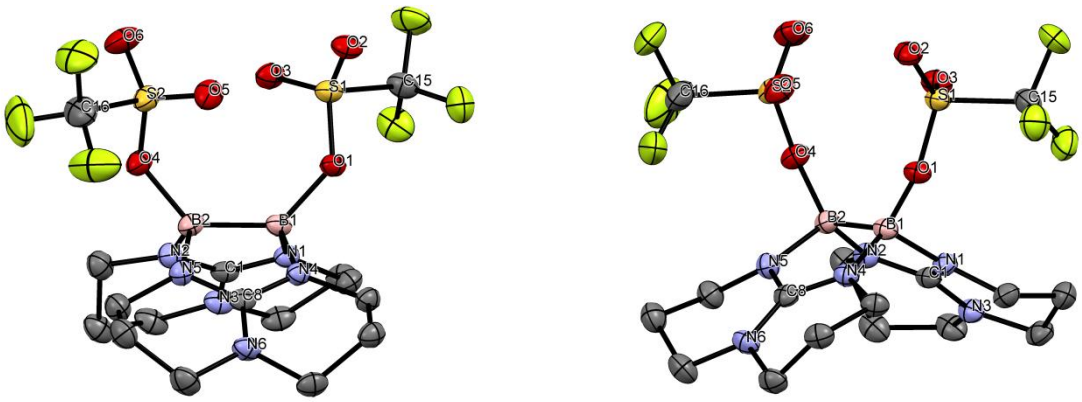

Figure S10. Structure of [TfOB(μ-hpp)]$_2$ from two perspectives. Displacement ellipsoids are shown at the 50 % probability level. Hydrogen atoms omitted for clarity. Selected bond distances (in Å) and angles (in °): B1−B2 1.708(4), B1−N1 1.5328(2), B1−N4 1.5403(2), B2−N2 1.5316(2), B2−N5 1.5362(2), N1−C1 1.3532(2), N2−C1 1.3401(2), N4−C8 1.3400(2), N5−C8 1.3524(2), C1−N3 1.3440(2), C8−N6 1.3481(2), B1−O1 1.5810(2), B2−O2 1.5769(2), O1−S1 1.4993(3), S1−O3 1.4237(2), S1−O4 1.4278(2), S1−C15 1.8237(4), O2−S2 1.4971(2), S2−O5 1.4201(2), S2−O6 1.4201(2), S2−C16 1.8135(3), O1−B1−B2 130.69(1), O2−B2−B1 130.459(10), N1−B1−N4 114.625(10), N2−B2−N5 114.552(10), N1−C1−N2 115.642(12), N4−C8−N5 115.628(12), O1−B1−B2−O2 9.3(4).

2) [PhCCB(μ-hpp)]$_2$ (5)

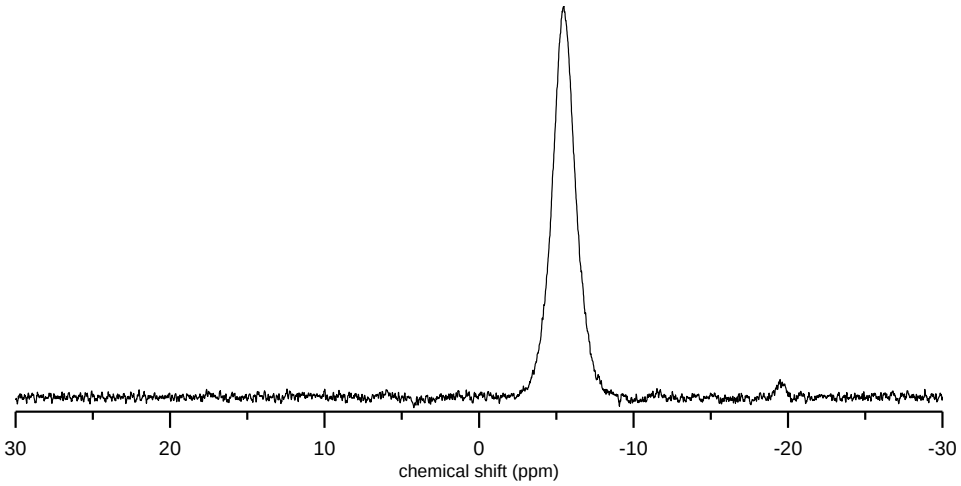

Figure S11. ^{11}B NMR spectrum (CD_2Cl_2, 128.30 MHz) for **5**.

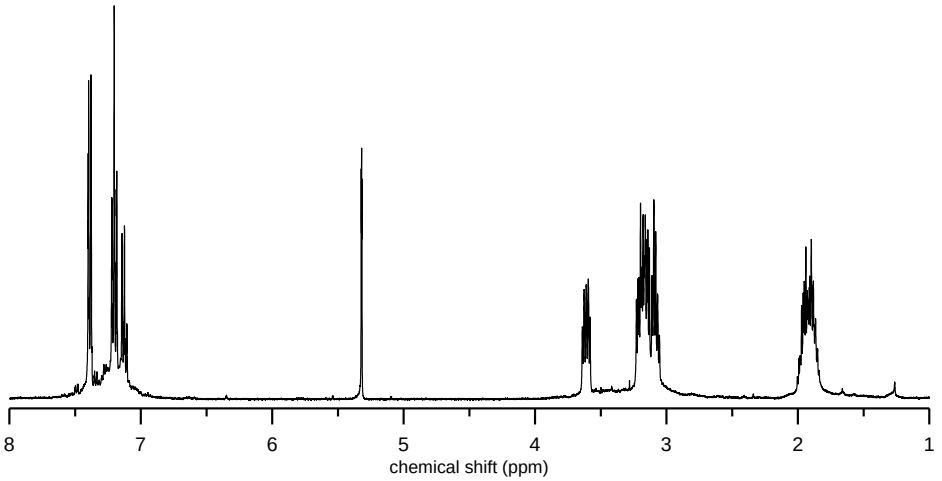

Figure S12. ^{1}H NMR spectrum (CD_2Cl_2, 399.89 MHz) for **5**.

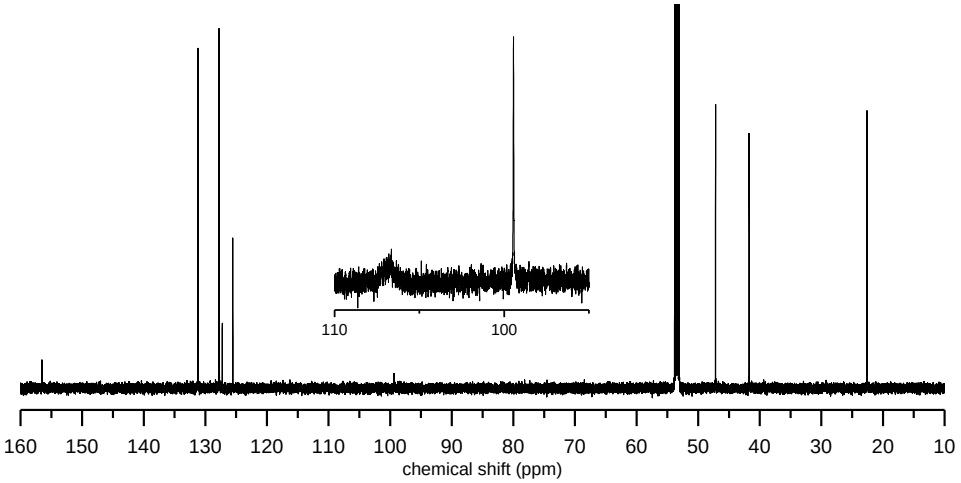

Figure S13. ^{13}C NMR spectrum (CD_2Cl_2, 150.92 MHz) for **5**, the inserted zoomed region was measured at 5 °C.

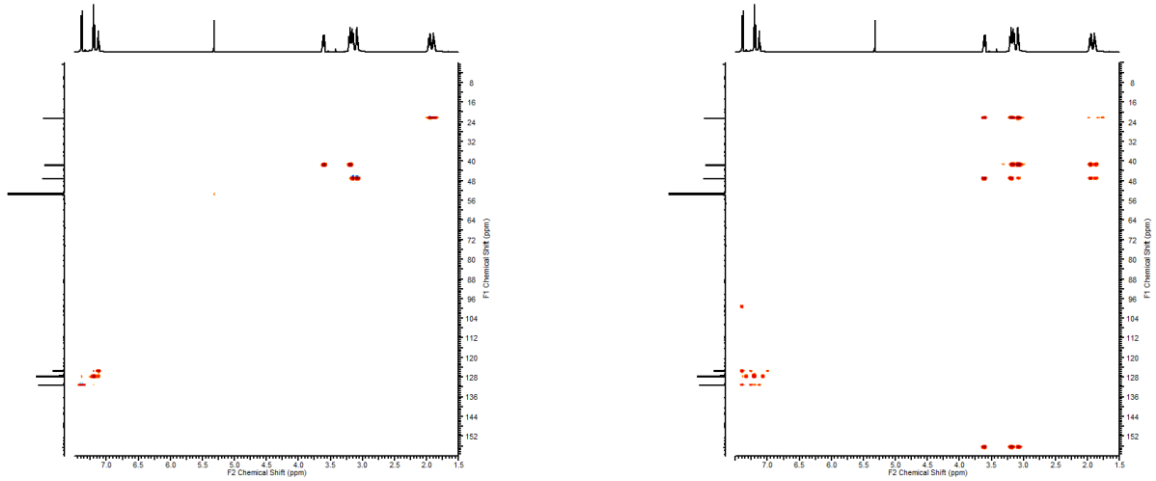

Figure S14. ^{1}H/^{13}C HSQC NMR spectrum (CD_2Cl_2, 600.13/150.92 MHz, left) and ^{1}H/^{13}C HMBC NMR spectrum (CD_2Cl_2, 600.13/150.92 MHz, right) for **5**.

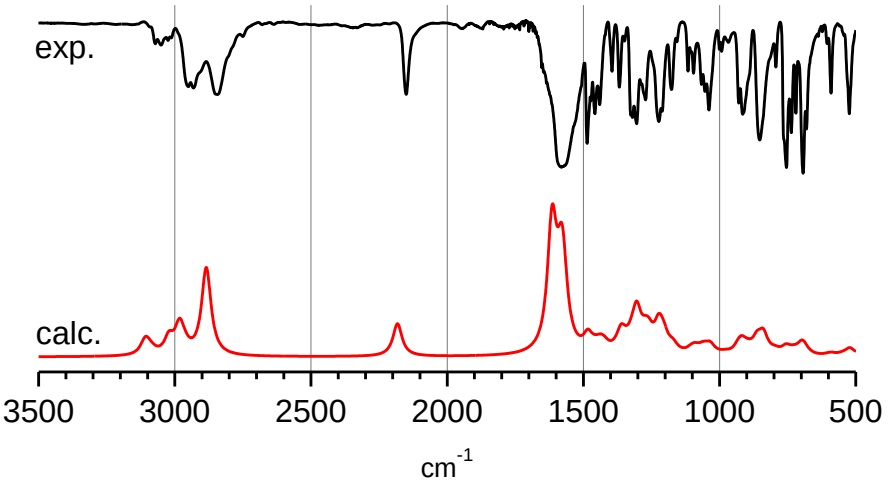

Figure S15. Experimental (KBr, top) and calculated (B3LYP-D3/def2-TZVPP, bottom) IR-spectra of **5**.

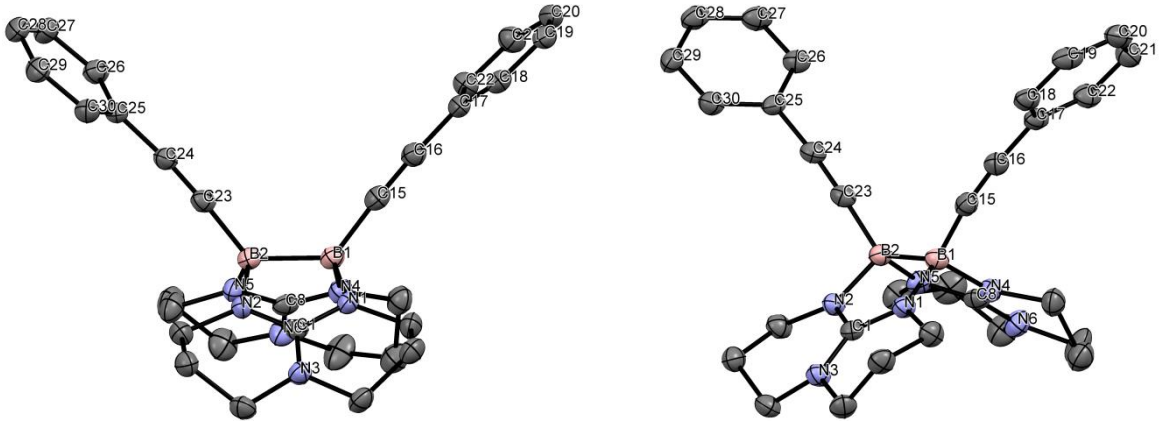

Figure S16. Structure of [PhCCB(μ-hpp)]$_2$ from two perspectives. Displacement ellipsoids are shown at the 50 % probability level. Hydrogen atoms omitted for clarity. Selected bond distances (in Å) and angles (in °): B1−B2 1.767(5), B1−N1 1.564(4), B1−N4 1.566(4), B2−N2 1.564(4), B2−N5 1.572(4), N1−C1 1.339(3), N2−C1 1.334(4), N4−C8 1.344(4), N5−C8 1.336(4), C1−N3 1.356(4), C8−N6 1.348 (4), B1−C15 1.581 (4), B2−C23 1.578(6), C15−C16 1.211(4), C16−C17 1.438(4), C17−C18 1.398(5), C17−C22 1.396(4), C18−C19 1.386(4), C21−C22 1.384(5), C20−C21 1.384(5), C19−C20 1.382(5), C23−C24 1.216(5), C24−C25 1.441(5), C25−C26 1.393(5), C25−C30 1.395(4), C26−C27 1.387(6), C27−C28 1.374(4), C29−C30 1.382(5), C28−C29 1.389(5), C15−B1−B2 127.7(3), C23−B2−B1 128.0(3), N1−B1−N4 111.6(2), N2−B2−N5 111.2(2), N1−C1−N2 115.2(2), N4−C8−N5 115.1(3), B1−C15−C16 171.9(3), C15−C16−C17 175.1(4), B2−C23−C24 177.0(3), C23−C24−C25 175.0(3), C15−B1−B2−C23 7.1(5).

3) [(*i*Pr)$_3$SiCCB(μ-hpp)]$_2$ (6)

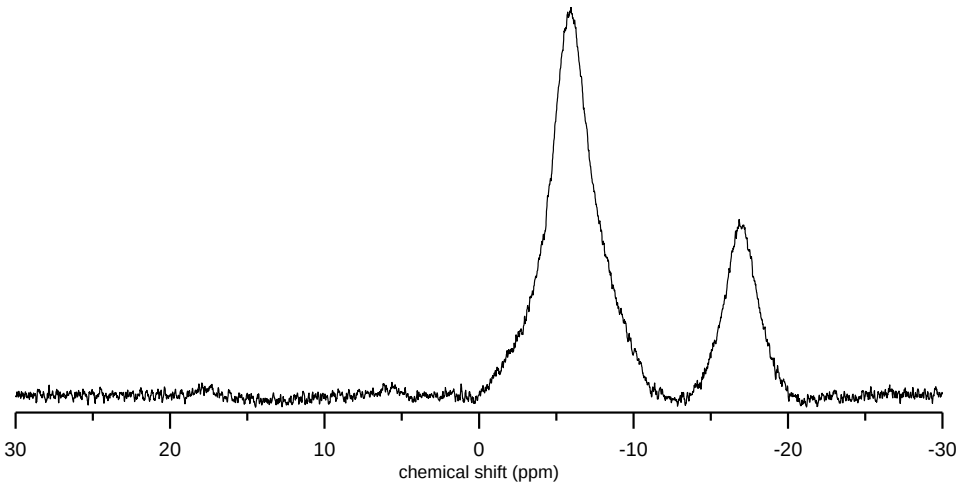

Figure S17. ^{11}B NMR spectrum (CD_2Cl_2, 128.30 MHz) for **6**.

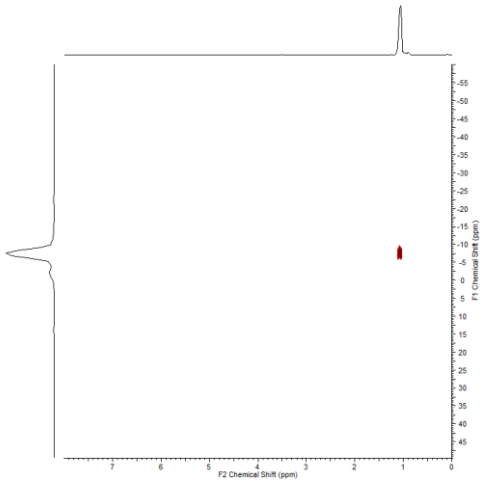

Figure S18. ^{1}H/^{29}Si HMBC spectrum (CD_2Cl_2, 399.89/79.44 MHz) for **6**.

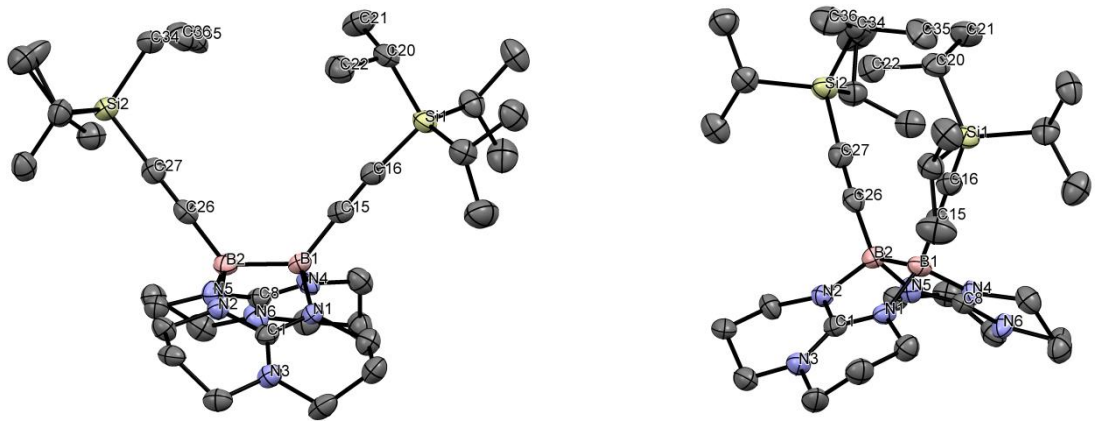

Figure S19. Structure of one of the two molecules per unit cell of [(*i*Pr)$_3$SiCCB(μ-hpp)]$_2$ (**6**) from two perspectives. Displacement ellipsoids are shown at the 50 % probability level.

Hydrogen atoms omitted for clarity. The corresponding values of the second molecule are marked with an apostrophe. Selected bond distances (in Å) and angles (in °): B1−B2 1.742(8), B1−N1 1.573(7), B1−N4 1.551(7), B2−N2 1.581(7), B2−N5 1.589(7), N1−C1 1.321(6), N2−C1 1.332(7), N4−C8 1.338(6), N5−C8 1.337(7), C1−N3 1.348(5), C8−N6 1,351(5), B1−C15 1.591(9), B2−C26 1.560(8), C15−C16 1.224(8), C16−Si1 1.811(6), Si1−C20 1.871(5), C20−C21 1.535(7), C20−C22 1.551(7), C26−C27 1.225(8), C27−Si2 1.832(5), Si2−C34 1.882(6), C34−C35 1.547(8), C34−C36 1.541(7), C15−B1−B2 126.5(5), C26−B2−B1 126.9(5), N1−B1−N4 110.6(4), N2−B2−N5 110.3(4), N1−C1−N2 115.8(4), N4−C8−N5 114.9(4), B1−C15−C16 177.2(6), C15−C16−Si1 174.5(5), B2−C26−C27 175.4(5), C26−C27−Si2 177.3(5), C15−B1−B2−C26 15.1(9);
B1'−B2' 1.761(8), B1'−N1' 1.585(7), B1'−N4' 1.572(7), B2'−N2' 1.564(7), B2'−N5' 1.575(7), N1'−C1' 1.340(7), N2'−C1' 1.342(7), N4'−C8' 1.352(7), N5'−C8' 1.341(5), C1'−N3' 1.361(6), C8'−N6' 1,341(5), B1'−C15' 1.562(9), B2'−C26' 1.598(9), C15'−C16' 1.214(9), C16'−Si1' 1.833(6), Si1'−C20' 1.865(6), C20'−C21' 1.540(9), C20'−C22' 1.547(9), C26'−C27' 1.221(8), C27'−Si2' 1.808(6), Si2'−C34' 1.902(5), C34'−C35' 1.523(8), C34'−C36' 1.537(8), C15'−B1'−B2' 127.0(5), C26'−B2'−B1' 124.2(5), N1'−B1'−N4' 109.9(4), N2'−B2'−N5' 111.2(4), N1'−C1'−N2' 116.0(4), N4'−C8'−N5' 115.3(4), B1'−C15'−C16' 176.7(6), C15'−C16'−Si1' 174.2(5), B2'−C26'−C27' 175.0(6), C26'−C27'−Si2' 174.3(5), C15'−B1'−B2'−C26' 14.2(8);

4) [MeOB(μ-hpp)]$_2$ (7)

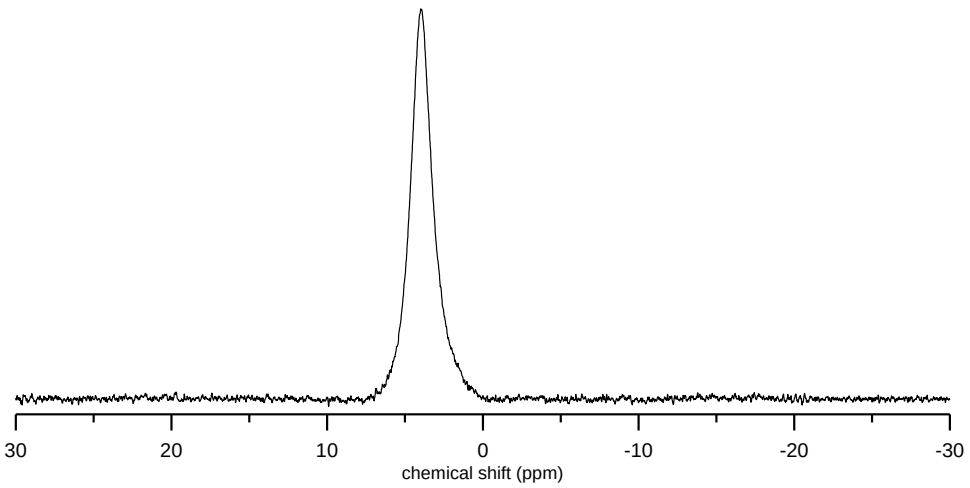

Figure S20. ^{11}B NMR spectrum (C_6D_6, 128.30 MHz) for **7**.

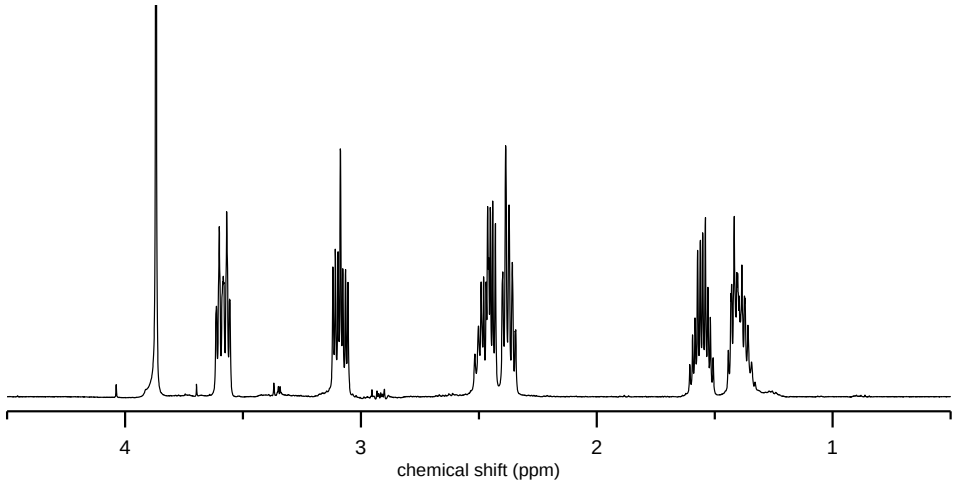

Figure S21. ^{1}H NMR spectrum (C_6D_6, 399.89 MHz) for **7**.

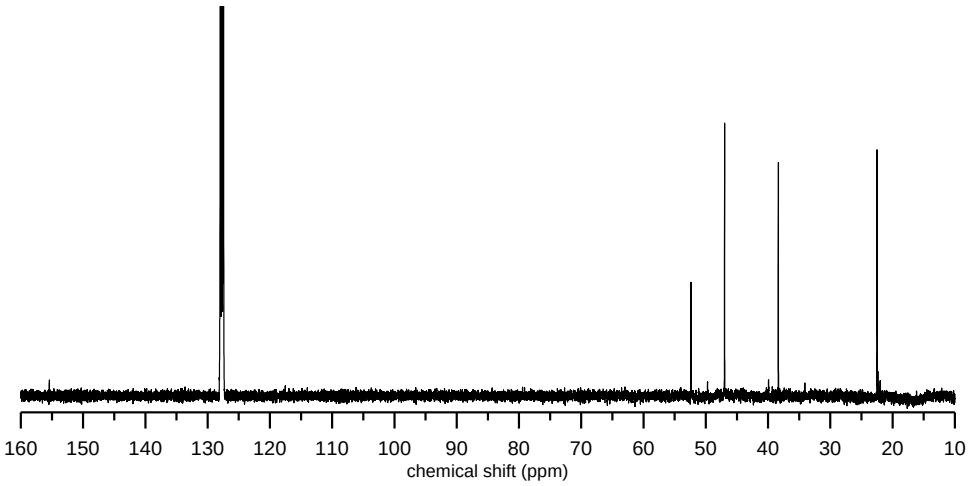

Figure S22. ^{13}C NMR spectrum (C_6D_6, 100.55 MHz) for **7**.

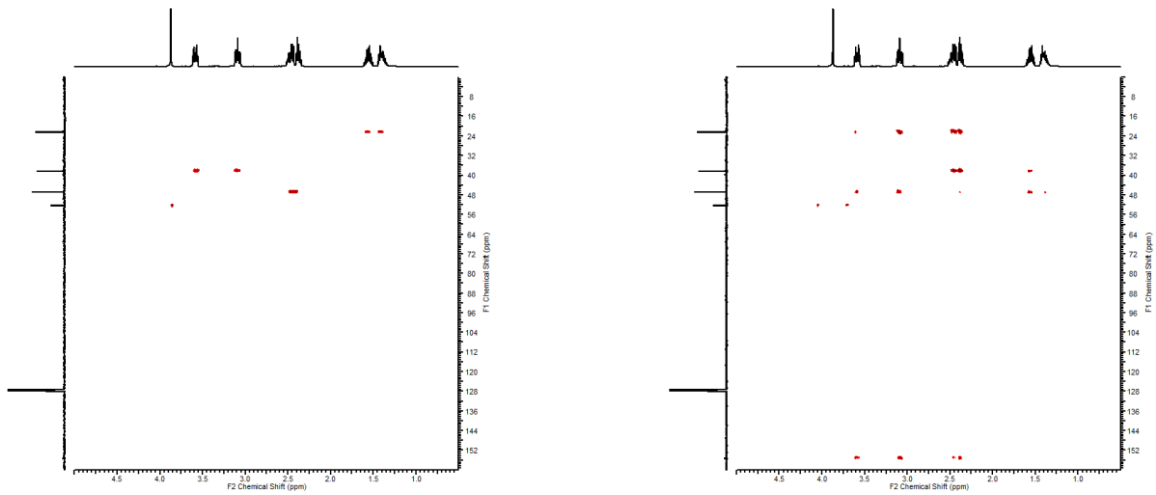

Figure S23. ^{1}H/^{13}C HSQC NMR spectrum (C_6D_6, 399.89/100.56 MHz, left) and ^{1}H/^{13}C HMBC NMR spectrum (C_6D_6, 399.89/100.56 MHz, right) for **7**.

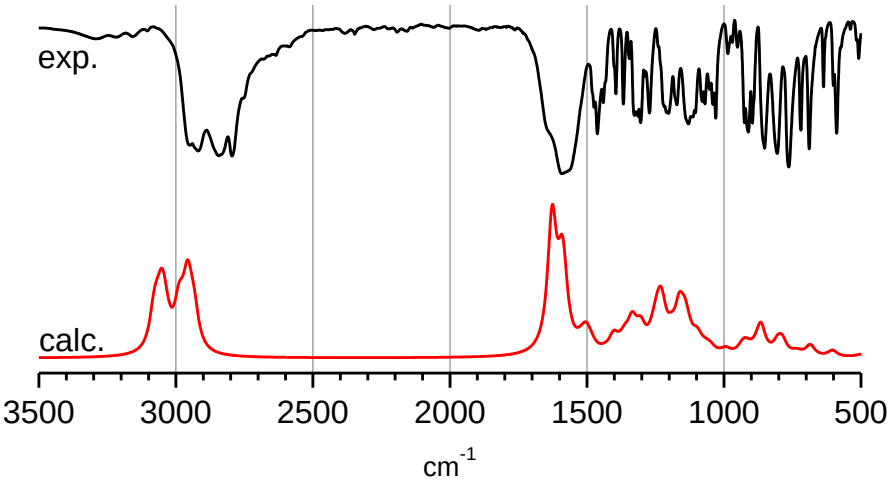

Figure S24. Experimental (KBr, top) and calculated (B3LYP-D3/def2-TZVPP, bottom) IR-spectra of **7**.

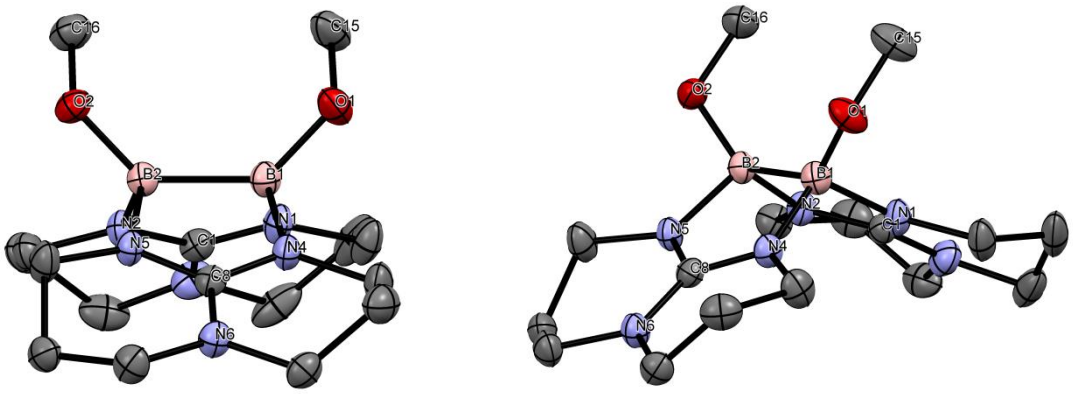

Figure S25. Structure of [MeOB(μ-hpp)]$_2$ from two perspectives. Displacement ellipsoids are shown at the 50 % probability level. Hydrogen atoms omitted for clarity. Selected bond distances (in Å) and angles (in °): B1−B2 1.773(2), B1−N1 1.587(2), B1−N4 1.560(2), B2−N2 1.594(2), B2−N5 1.563(2), N1−C1 1.336(2), N2−C1 1.337(2), N4−C8 1.343(2), N5−C8 1.343(2), C1−N3 1.363(2), C8−N6 1.352(2), B1−O1 1.463(2), B2−O2 1.465(2), O1−C15 1.402(2), O2−C16 1.400(2), O1−B1−B2 132.4(1), O2−B2−B1 133.6(1), N1−B1−N4 110.8(1), N2−B2−N5 111.4(1), N1−C1−N2 115.6(1), N4−C8−N5 115.2(1), B1−O1−C15 116.6(1), B2−O2−C16 117.4(1), O1−B1−B2−O2 3.4(2).

5) $[Me_2NB(\mu\text{-hpp})]_2$ (8)

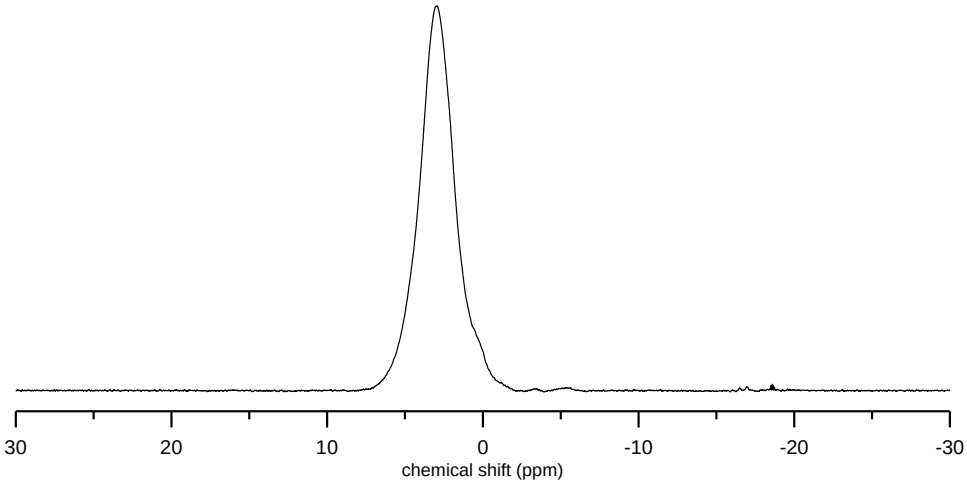

Figure S26. ^{11}B NMR spectrum (d_8-Toluol, 128.30 MHz) for **8**.

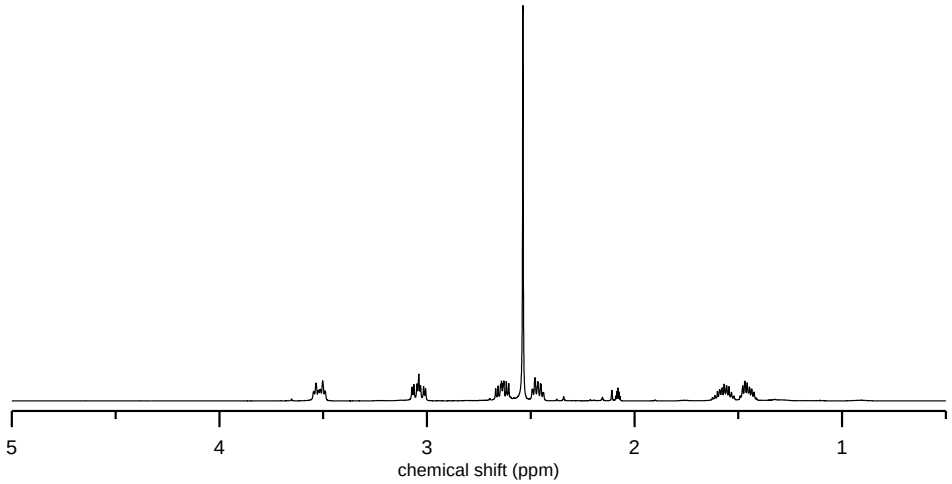

Figure S27. ^{1}H NMR spectrum (d_8-Toluol, 399.89 MHz) for **8**.

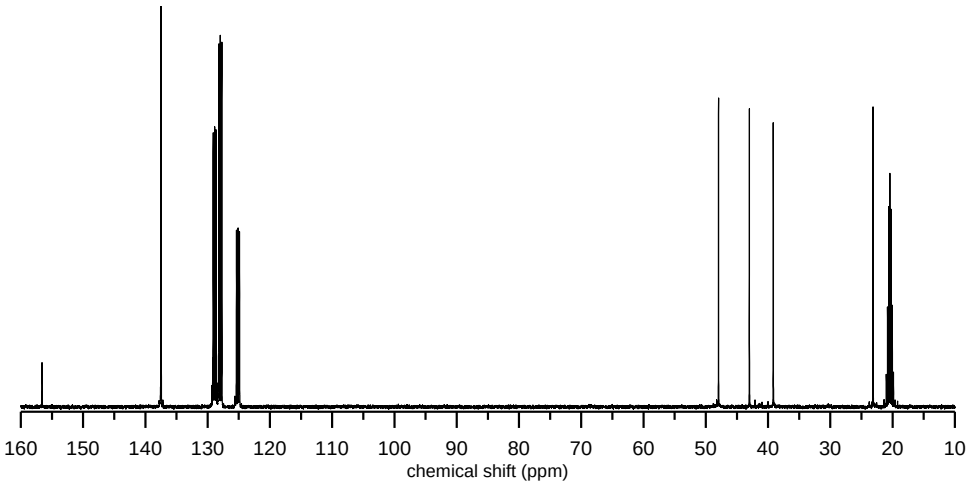

Figure S28. ^{13}C NMR spectrum (d_8-Toluol, 100.55 MHz) for **8**.

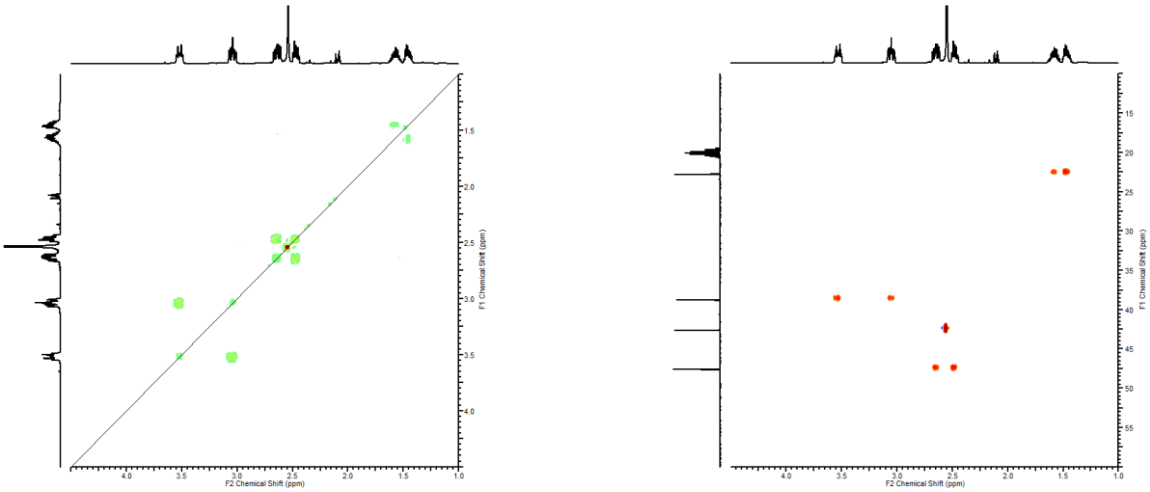

Figure S29. $^{1}H/^{1}H$ COSY NMR spectrum (d_8-Toluol, 399.89/399.89 MHz, left) and $^{1}H/^{13}C$ HSQC NMR spectrum (d_8-Toluol, 399.89/100.56 MHz, right) for **8**.

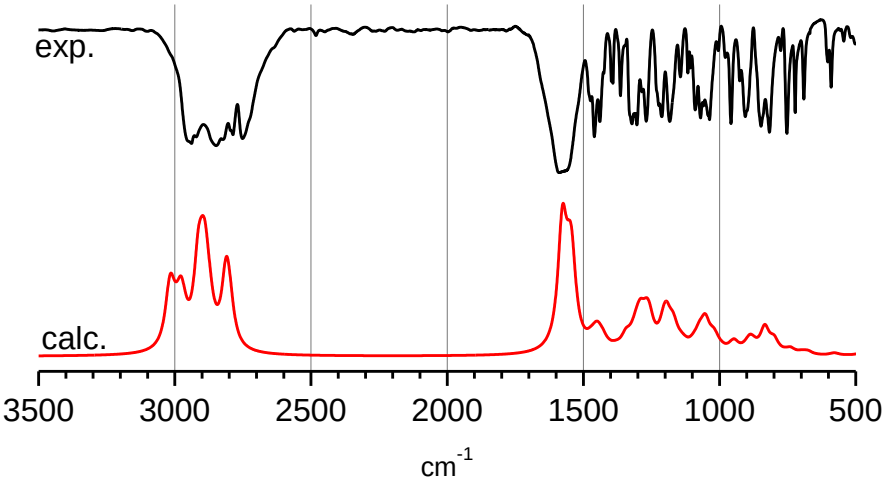

Figure S30. Experimental (KBr, top) and calculated (B3LYP-D3/def2-TZVPP, bottom) IR-spectra of **8**.

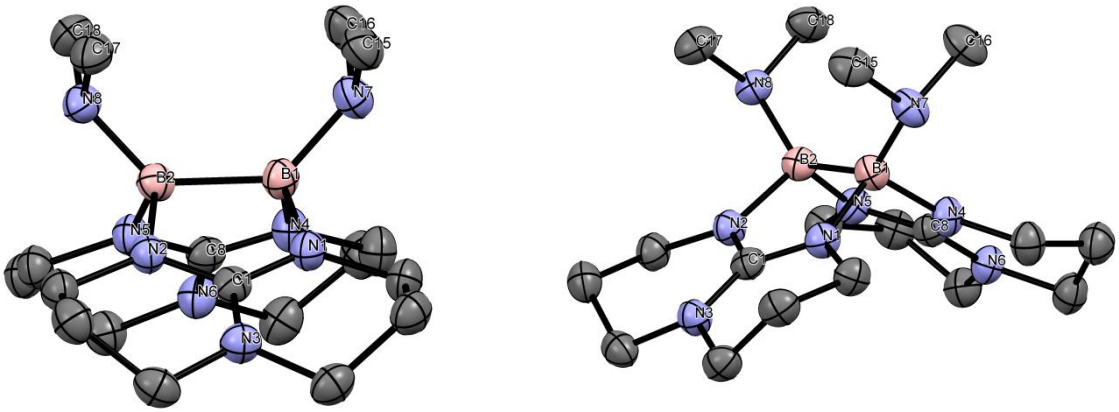

Figure S31. Structure of $[Me_2NB(\mu\text{-hpp})]_2$ from two perspectives. Displacement ellipsoids are shown at the 50 % probability level. Hydrogen atoms omitted for clarity. Selected bond distances (in Å) and angles (in °): B1−B2 1.766(3), B1−N1 1.586(3), B1−N4 1.589(2),

B2−N2 1.577(3), B2−N5 1.574(2), N1−C1 1.345(2), N2−C1 1.337(2), N4−C8 1.340(2), N5−C8 1.574(2), C1−N3 1.355(2), C8−N6 1.360(2), B1−N7 1.534(2), B2−N8 1.536(2), N7−C15 1.448(3), N7−C16 1.445(3), N8−C17 1.447(2), N8−C18 1.451(3), N7−B1−B2 132.9(2), N8−B2−B1 131.7(2), N1−B1−N4 110.3(1), N2−B2−N5 109.8(1), N1−C1−N2 115.2(1), N4−C8−N5 115.5(1), C15−N7−C16 109.6(1), C17−N8−C18 109.4(1), N7−B1−B2−N8 1.0(3), B1−B2−N8−C17 −63.9(2), B1−B2−N8−C18 64.8(2), B2−B1−N7−C15 65.0(2), B2−B1−N7−C16 −65.6(2).

Summary of quantum chemical computations

Table S1. Correlations between experimental and calculated ^{11}B NMR chemical shifts. Referenced to the experimental NMR shift of [HB(μ-hpp)]$_2$ (**1**).

	$\delta(^{11}B)$/ppm exp.	$\delta(^{11}B)$/ppm BP86-D3 /def2-SV(P)	$\delta(^{11}B)$/ppm BP86-D3 /def2-TZVPP	$\delta(^{11}B)$/ppm B3LYP-D3 /def2-TZVPP
[TfOB(μ-hpp)]$_2$ (**4**)	5.08	3.91	5.15	5.70
[ClB(μ-hpp)]$_2$ (**9**)	3.64	4.09	5.45	5.28
{[Me$_2$HNB(μ-hpp)]$_2$}$^{2+}$ (**3**)	1.33	2.21	3.29	3.14
[*n*BuB(μ-hpp)]$_2$ (**10**)	−1.39	−2.40	−1.46	−1.15
[PhCCB(μ-hpp)]$_2$ (**5**)	−5.50	−4.26	−4.37	−4.05
[(*i*Pr)$_3$SiCCB(μ-hpp)]$_2$ (**6**)	−5.75	−4.49	−4.93	−4.54
[HB(μ-hpp)]$_2$ (**1**)	−2.45	−2.45	−2.45	−2.45
[Me$_2$NB(μ-hpp)]$_2$ (**8**)	1.56	0.34	1.26	2.18
[MeOB(μ-hpp)]$_2$ (**7**)	3.35	2.48	3.92	4.12

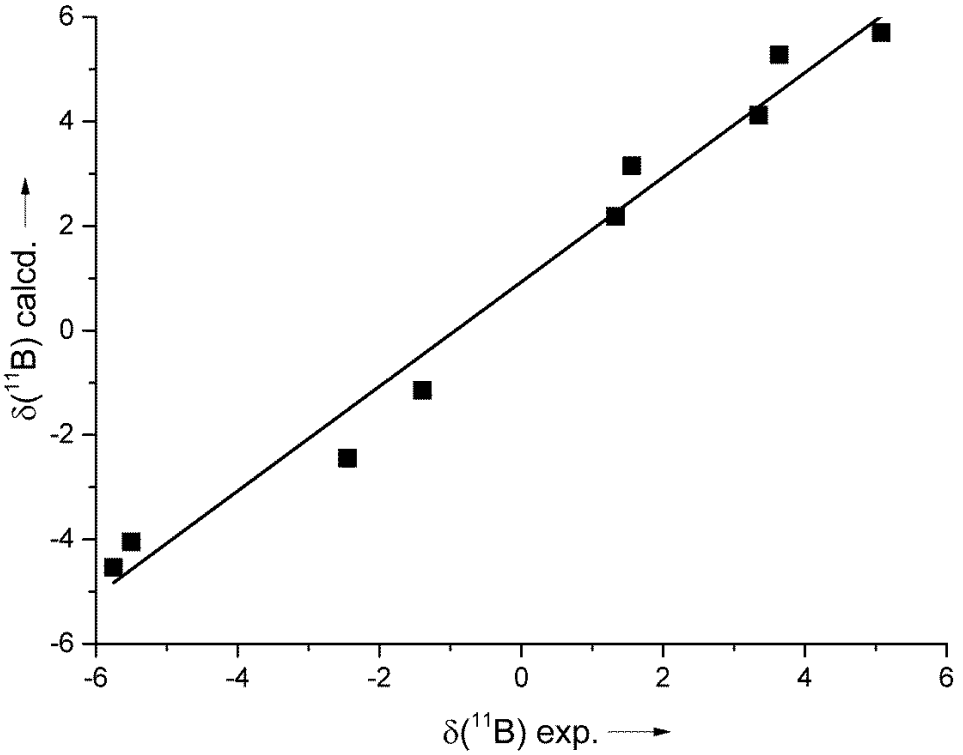

Figure S32. Correlation between exp. ^{11}B NMR chemical shifts and values calculated with B3LYP-D3/def2-TZVPP (linear fit with R = 0.98924).

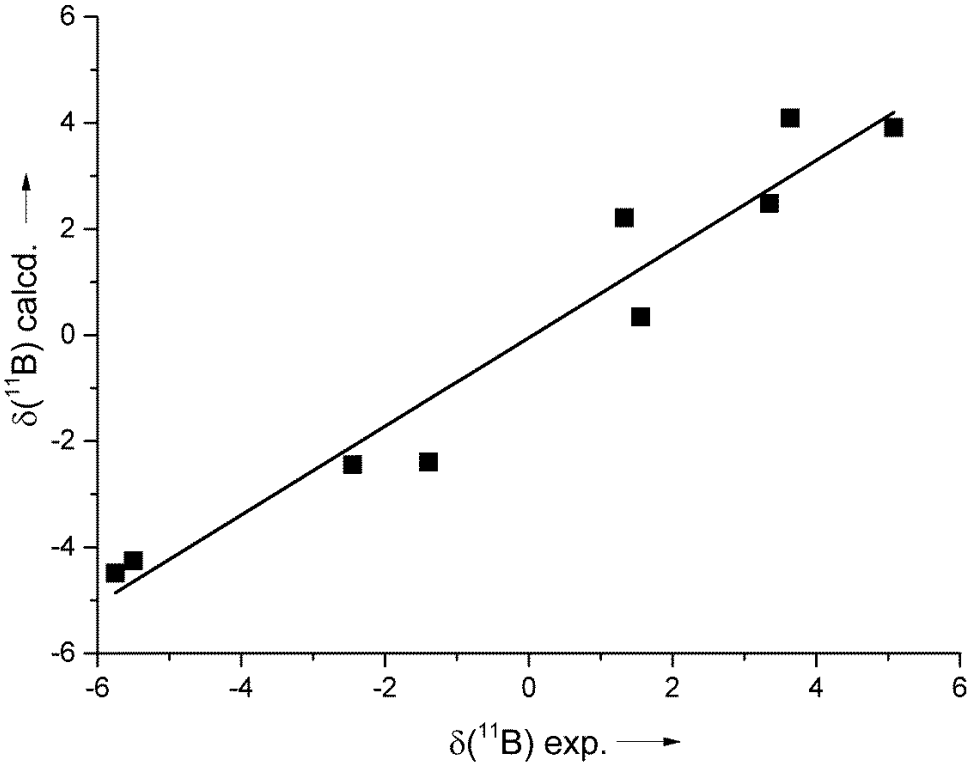

Figure S33. Correlation between exp. ^{11}B NMR chemical shifts and values calculated with BP86-D3/def2-SV(P) (linear fit with R = 0.97097).

Table S2. Correlations between experimental and calculated B-B bond lengths.

	B-B/Å exp.	B-B/Å BP86-D3 /def2-SV(P)	B-B/Å BP86-D3 /def2-TZVPP	B-B/Å B3LYP-D3 /def2-TZVPP
$[TfOB(\mu\text{-hpp})]_2$ (**4**)	1.708(4)	1.724	1.715	1.706
$[ClB(\mu\text{-hpp})]_2$ (**9**)	1.710(3)	1.744	1.734	1.724
$\{[Me_2HNB(\mu\text{-hpp})]_2\}^{2+}$ (**3**)	1.746(2)	1.761	1.761	1.748
$[n\text{BuB}(\mu\text{-hpp})]_2$ (**10**)	1.755(3)	1.770	1.761	1.753
$[PhCCB(\mu\text{-hpp})]_2$ (**5**)	1.759(3)	1.784	1.775	1.760
$[(i\text{Pr})_3SiCCB(\mu\text{-hpp})]_2$ (**6**)	1.761(8)/ 1.742(8)	1.770	1.762	1.751
$[HB(\mu\text{-hpp})]_2$ (**1**)	1.772(3)	1.759	1.749	1.742
$[Me_2NB(\mu\text{-hpp})]_2$ (**8**)	1.766(3)	1.764	1.758	1.750
$[MeOB(\mu\text{-hpp})]_2$ (**7**)	1.773(2)	1.753	1.750	1.750

Table S3. Root-Mean-Square Deviation (RMSD) between calculated and experimental structures.

	RMSD BP86-D3 /def2-SV(P)	RMSD BP86-D3 /def2-TZVPP	RMSD B3LYP-D3 /def2-TZVPP
$[TfOB(\mu\text{-hpp})]_2$ (**4**)	0.4191	0.4828	0.4834
$[ClB(\mu\text{-hpp})]_2$ (**9**)	0.3625	0.4354	0.4348
$\{[Me_2HNB(\mu\text{-hpp})]_2\}^{2+}$ (**3**)	0.3949	0.4041	0.4129
$[n\text{BuB}(\mu\text{-hpp})]_2$ (**10**)	0.3292	0.2432	0.2483
$[PhCCB(\mu\text{-hpp})]_2$ (**5**)	0.3431	0.3399	0.3438
$[(i\text{Pr})_3SiCCB(\mu\text{-hpp})]_2$ (**6**)	0.2950/0.3265	0.2939/0.3270	0.2941/0.3216
$[HB(\mu\text{-hpp})]_2$ (**1**)	0.5103	0.4299	0.4198
$[Me_2NB(\mu\text{-hpp})]_2$ (**8**)	0.2668	0.2526	0.2546
$[MeOB(\mu\text{-hpp})]_2$ (**7**)	0.2662	0.2676	0.2478
Average	0.3514	0.3476	0.3461

Table S4. Comparison between some calculated (B3LYP-D3/def2-TZVPP) parameters (extended version of Table 2 in the main text). Values for proton affinity are relative to $[HB(\mu\text{-hpp})]_2$ (**1**).

	q / e	ρ / e Å^{-3}	E(HOMO) / eV	I_1 / kJ mol^{-1}	ΔPA / kJ mol^{-1}
$[Me_2NB(\mu\text{-hpp})]_2$ (**8**)	0.529	1.523	−3.492	375.60	+72.21
$[n\text{BuB}(\mu\text{-hpp})]_2$ (**10**)	0.380	1.474	−4.649	450.42	+41.78
$[\text{MeOB}(\mu\text{-hpp})]_2$ (**7**)	0.579	1.518	−4.242	471.87	+12.32
$[HB(\mu\text{-hpp})]_2$ (**1**)	0.155	1.485	−4.780	536.07	0
$[\text{PhCCB}(\mu\text{-hpp})]_2$ (**5**)	0.301	1.413	−4.617	518.58	−52.82
$[(i\text{Pr})_3\text{SiCCB}(\mu\text{-hpp})]_2$ (**6**)	0.293	1.441	−4.832	529.25	−58.37
$[\text{ClB}(\mu\text{-hpp})]_2$ (**9**)	0.344	1.586	−5.124	574.35	−92.71
$[\text{TfOB}(\mu\text{-hpp})]_2$ (**4**)	0.583	1.665	−6.145	575.25	−97.35
$\{[Me_2HNB(\mu\text{-hpp})]_2\}^{2+}$ (**3**)	0.537	1.462	−11.915	1271.70	−742.68
B_2Cl_4	0.189	1.664	−8.205	942.17	−460.35
$B_2Cl_4(NMe_3)_2$	0.251	1.433	−6.444	691.38	−184.27
$B_2Cl_4(NHMe_2)_2$	0.184	1.540	−6.489	711.10	−245.59

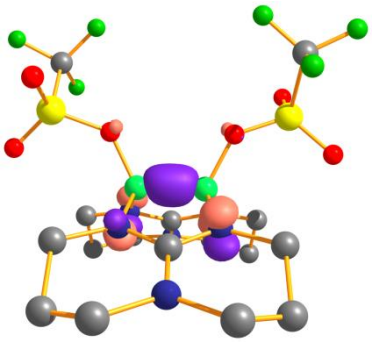

[TfOB(μ-hpp)]$_2$ (**4**)

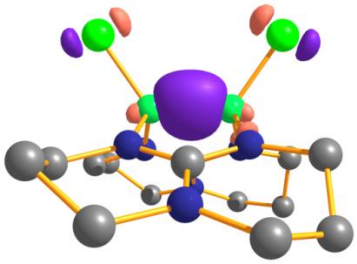

[ClB(μ-hpp)]$_2$ (**9**)

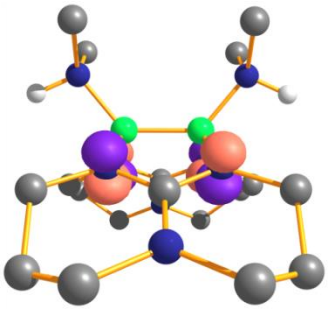

{[Me$_2$HNB(μ-hpp)]$_2$}$^{2+}$ (**3**)

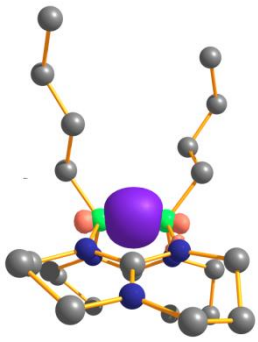

[*n*BuB(μ-hpp)]$_2$ (**10**)

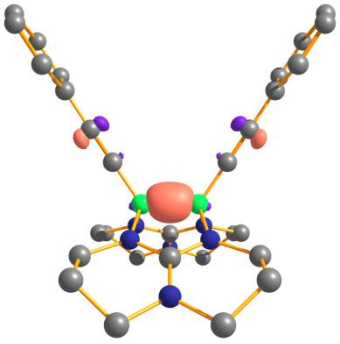

[PhCCB(μ-hpp)]$_2$ (**5**)

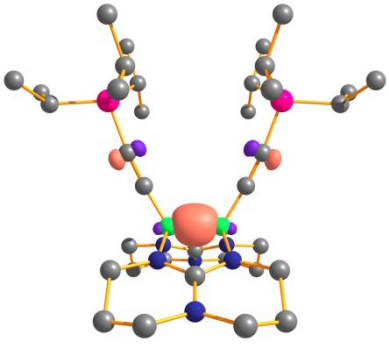

[(*i*Pr)$_3$SiCCB(μ-hpp)]$_2$ (**6**)

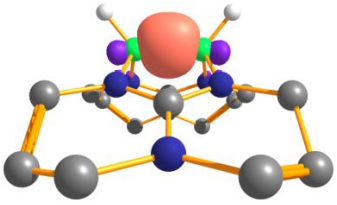

[HB(μ-hpp)]$_2$ (**1**)

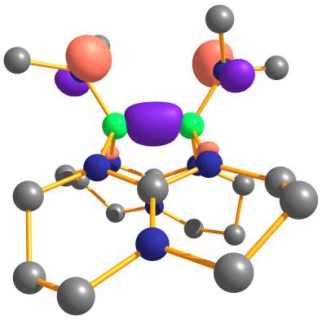

[Me$_2$NB(μ-hpp)]$_2$ (**8**)

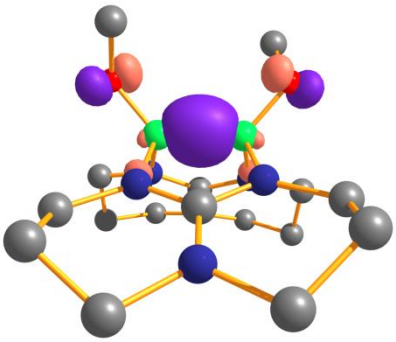

[MeOB(μ-hpp)]$_2$ (**7**)

Figure S34. Illustrations of the isodensity surfaces (contour value 0.1) for the HOMOs in the diboranes discussed in this work. Carbon-bound hydrogen atoms omitted for clarity.

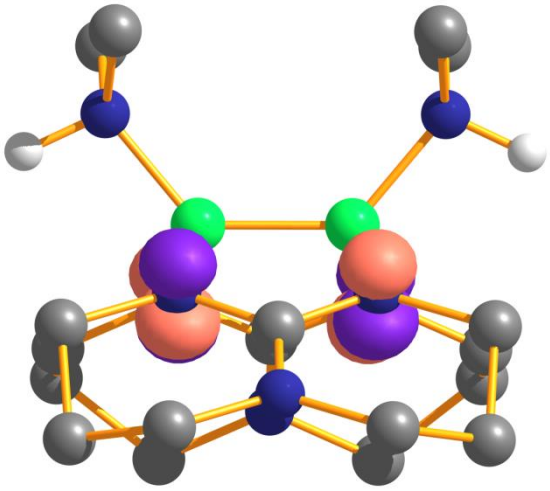

HOMO (−11.916 eV)

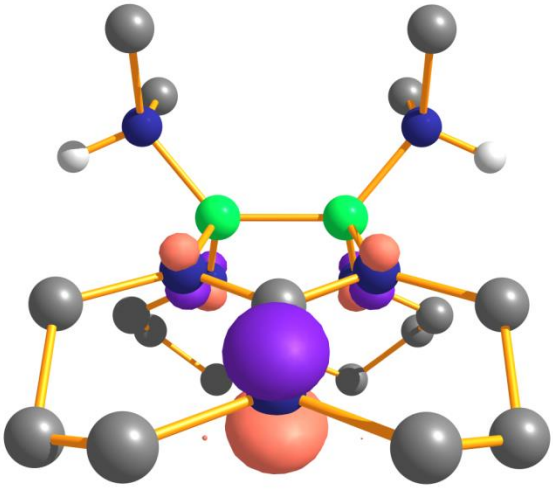

HOMO−1 (−12.231 eV)

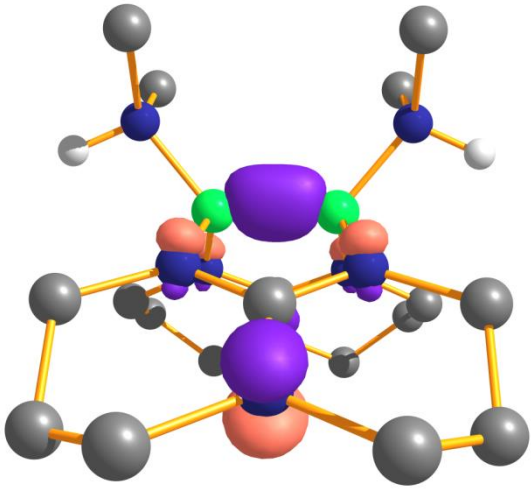

HOMO−2 (−12.368 eV)

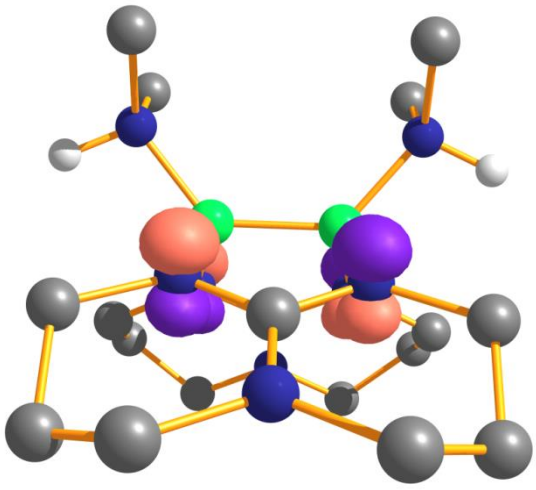

HOMO−3 (−12.717 eV)

Figure S35. Illustrations of the isodensity surfaces (contour value 0.1) for the HOMO to HOMO−3 of $\{[Me_2HNB(\mu\text{-hpp})]_2\}^{2+}$ (**3**) and the corresponding orbital energy. Carbon-bound hydrogen atoms omitted for clarity.

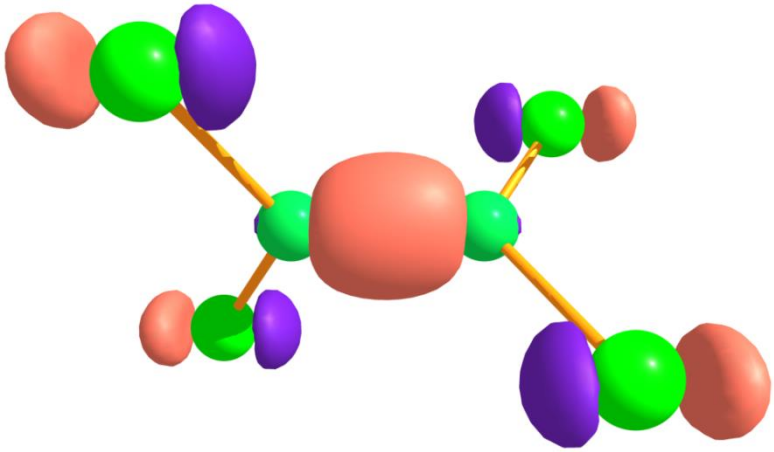

Figure S36. Illustrations of the isodensity surfaces (contour value 0.1) for the HOMO of B_2Cl_4.

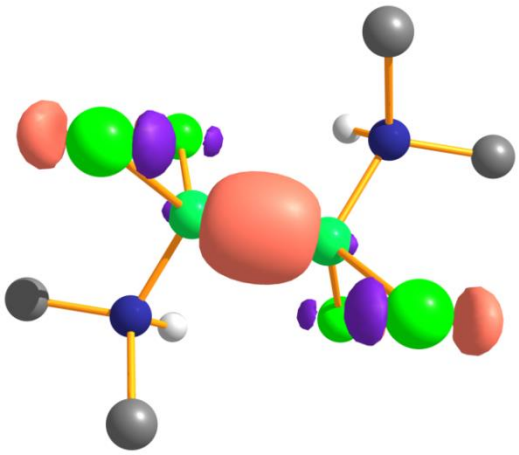

Figure S37. Illustrations of the isodensity surfaces (contour value 0.1) for the HOMO of $B_2Cl_4(NHMe_2)_2$. Carbon-bound hydrogen atoms omitted for clarity.

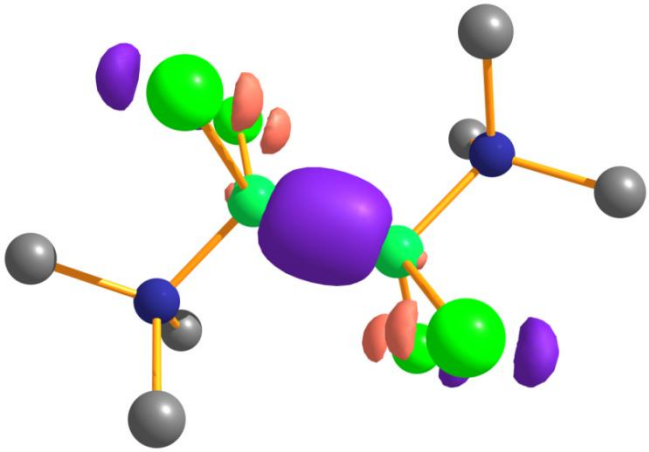

Figure S38. Illustrations of the isodensity surfaces (contour value 0.1) for the HOMO of $B_2Cl_4(NMe_3)_2$. Hydrogen atoms omitted for clarity.

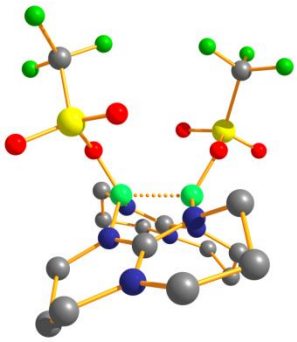

[TfOB(μ-hpp)]$_2^{\bullet+}$ (**4**$^{\bullet+}$)

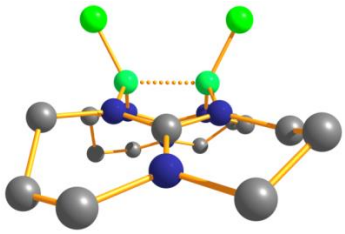

[ClB(μ-hpp)]$_2^{\bullet+}$ (**9**$^{\bullet+}$)

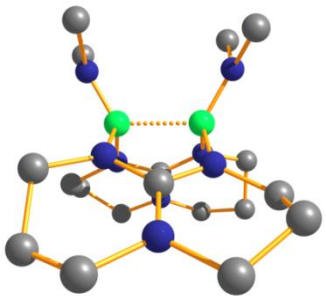

[Me_2NB(μ-hpp)]$_2^{\bullet+}$ (**3**$^{\bullet+}$)

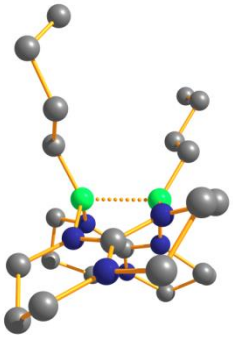

[*n*BuB(μ-hpp)]$_2^{\bullet+}$ (**10**$^{\bullet+}$)

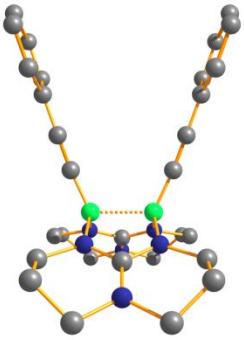

[PhCCB(μ-hpp)]$_2^{\bullet+}$ (**5**$^{\bullet+}$)

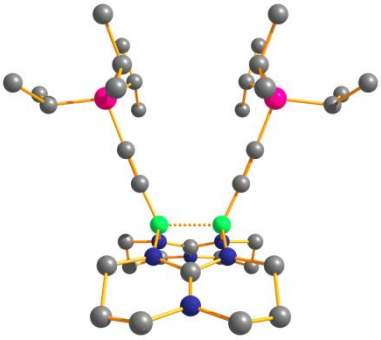

[TIPSCCB(μ-hpp)]$_2^{\bullet+}$ (**6**$^{\bullet+}$)

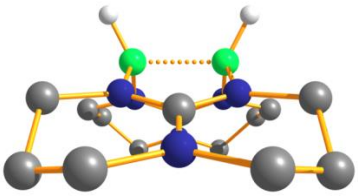

[HB(μ-hpp)]$_2^{\bullet+}$ (**1**$^{\bullet+}$)

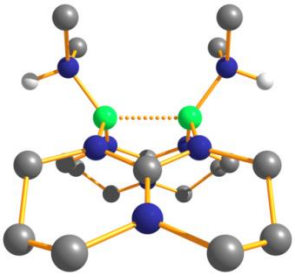

[Me_2HNB(μ-hpp)]$_2^{\bullet 3+}$ (**3**$^{\bullet+}$)

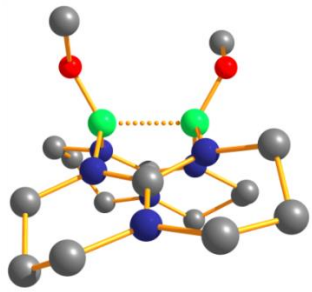

[MeOB(μ-hpp)]$_2^{\bullet+}$ (**7**$^{\bullet+}$)

Figure S39. Illustration of the radical cationic diboranes obtained upon one-electron oxidation of the neutral diboranes (used for determination of the ionization energy). Carbon-bound hydrogen atoms omitted for clarity.

Table S6. Comparison of the B-B bond distances in the diboranes before and after one-electron oxidation (calculated values computed with B3LYP-D3/def2-TZVPP).

	neutral		monocationic
	B-B/Å exp.	B-B/Å calcd.	B-B/Å calcd.
[TfOB(μ-hpp)]$_2$ (**4**)	1.708(4)	1.706	1.969
[ClB(μ-hpp)]$_2$ (**9**)	1.710(3)	1.724	2.072
{[Me$_2$HNB(μ-hpp)]$_2$}$^{2+}$ (**3**)	1.746(2)	1.748	2.172
[*n*BuB(μ-hpp)]$_2$ (**10**)	1.755(3)	1.753	2.044
[PhCCB(μ-hpp)]$_2$ (**5**)	1.759(3)	1.760	2.062
[(*i*Pr)$_3$SiCCB(μ-hpp)]$_2$ (**6**)	1.761(8)/1.742(8)	1.751	2.091
[HB(μ-hpp)]$_2$ (**1**)	1.772(3)	1.742	2.093
[Me$_2$NB(μ-hpp)]$_2$ (**8**)	1.766(3)	1.750	2.003
[MeOB(μ-hpp)]$_2$ (**7**)	1.773(2)	1.750	2.019

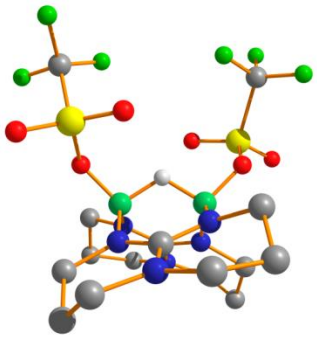

{[TfOB(μ-hpp)]$_2$H}$^+$ (**4**+H)$^+$

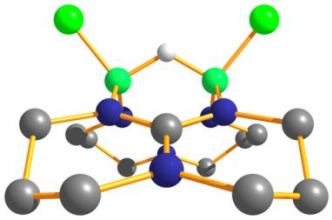

{[ClB(μ-hpp)]$_2$H}$^+$ (**9**+H)$^+$

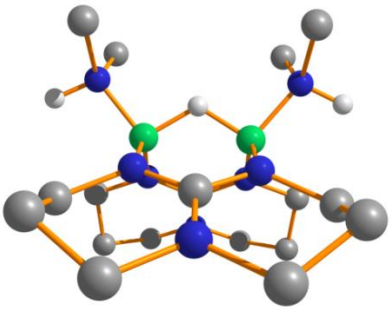

{[Me$_2$HNB(μ-hpp)]$_2$H}$^{3+}$ (**3**+H)$^+$

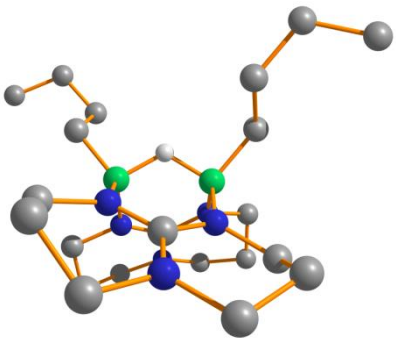

{[*n*BuB(μ-hpp)]$_2$H}$^+$ (**10**+H)$^+$

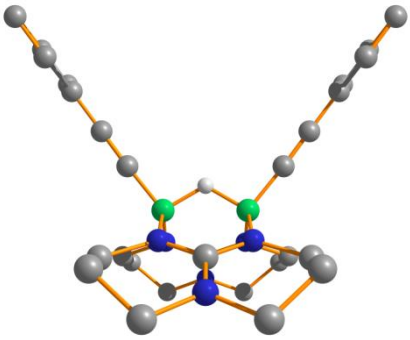

{[PhCCB(μ-hpp)]$_2$H}$^+$ (**5**+H)$^+$

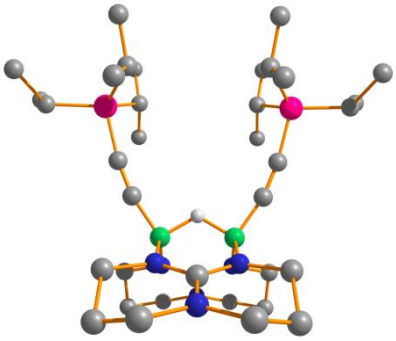

{[TIPSCCB(μ-hpp)]$_2$H}$^+$ (**6**+H)$^+$

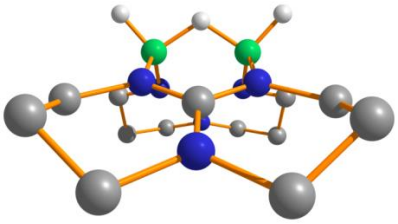

{[HB(μ-hpp)]$_2$H}$^+$ (**1**+H)$^+$

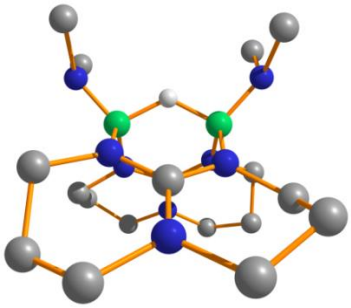

{[Me$_2$NB(μ-hpp)]$_2$H}$^+$ (**8**+H)$^+$

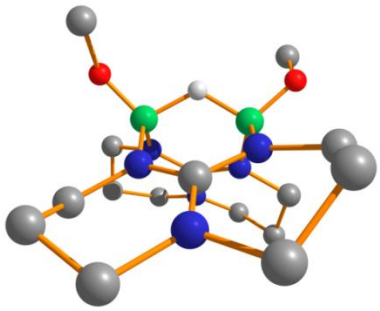

$\{[MeOB(\mu\text{-hpp})]_2H\}^+$ (**7**+H)$^+$

Figure S40. Illustration of the structures calculated for the protonated diboranes (B3LYP-D3/def2-TZVPP computations). Carbon-bound hydrogen atoms omitted.

Table S7. Comparison of the B-B distances in the diboranes before and after protonation of the B-B bond (Calculated values computed with B3LYP-D3/def2-TZVPP).

	$[XB(\mu\text{-hpp})]_2$		$\{[XB(\mu\text{-hpp})]_2+H\}^+$
	B-B/Å exp.	B-B/Å calcd.	B-B/Å calcd.
$[TfOB(\mu\text{-hpp})]_2$ (**4**)	1.708(4)	1.706	2.237
$[ClB(\mu\text{-hpp})]_2$ (**9**)	1.710(3)	1.724	2.249
$\{[Me_2HNB(\mu\text{-hpp})]_2\}^{2+}$ (**3**)	1.746(2)	1.748	2.262
$[n\text{BuB}(\mu\text{-hpp})]_2$ (**10**)	1.755(3)	1.753	2.255
$[PhCCB(\mu\text{-hpp})]_2$ (**5**)	1.759(3)	1.760	2.274
$[(i\text{Pr})_3SiCCB(\mu\text{-hpp})]_2$ (**6**)	1.761(8)/1.742(8)	1.751	2.260
$[HB(\mu\text{-hpp})]_2$ (**1**)	1.772(3)	1.742	2.203*
$[Me_2NB(\mu\text{-hpp})]_2$ (**8**)	1.766(3)	1.750	2.359
$[MeOB(\mu\text{-hpp})]_2$ (**7**)	1.773(2)	1.750	2.333

*Experimentally derived structure: 2.229(4) Å